Hindawi
Journal of Nanotechnology
Volume 2019, Article ID 1895043, 11 pages
https://doi.org/10.1155/2019/1895043

Research Article

Highly Efficient Photocatalysis by Zinc Oxide-Reduced Graphene Oxide (ZnO-rGO) Composite Synthesized via One-Pot Room-Temperature Chemical Deposition Method

Roselle T. Ngaloy,[1] **Aixeen M. Fontanilla**,[1] **Ma. S. Rebecca Soriano**,[1] **Chelo S. Pascua**,[1] **Yoshitaka Matsushita**,[2] **and Ian Jasper A. Agulo**[1]

[1]*Micro and Nano Innovations Laboratory, Department of Physical Sciences, College of Science, University of the Philippines Baguio, Baguio 2600, Philippines*
[2]*Materials Analysis Station, National Institute for Materials Science, Sengen, Tsukuba, Ibaraki 305-0047, Japan*

Correspondence should be addressed to Roselle T. Ngaloy; rtngaloy@up.edu.ph

Received 28 August 2019; Accepted 26 November 2019; Published 24 December 2019

Academic Editor: Tomonori Ohba

We synthesized zinc oxide-reduced graphene oxide (ZnO-rGO) composites using a one-pot chemical deposition method at room temperature. Zinc powder and graphene oxide (GO) of different mass ratios (1 : 1, 1 : 2, 1 : 5, 1 : 10, and 1 : 20 GO to Zn) were used as precursors in a mildly alkaline solution. UV-Vis spectroscopy was used to study the photocatalytic efficiency of the samples through the photodegradation of methylene blue (MB). UV-Vis measurements show the fast decomposition of methylene blue under UV light illumination with the best degradation efficiency of 97.7% within one hour, achieved with sample ZG2 (1 GO : 2 Zn mass ratio). The corresponding degradation rate was $k_{ZG2} = 0.1253\ min^{-1}$, which is at least 5.5 times better than other existing works using hydrothermal methods. We argue that the excellent photodegradation of MB by ZG2 is due to the efficient charge separation brought about by the electronic interaction of the rGO with the ZnO and the formation of a Zn-O-C bond, as supported by XRD and Raman spectroscopy measurements.

1. Introduction

The discovery of new materials has led to the development of various applications in the field of environmental remediation. Among the immediate concern for remediation is the treatment of pollutants in waterways and bodies of water as increasing awareness to limited water resources arise. Methylene blue (MB) is one of the most extensively researched dyes for photodegradation. MB dye is used in textile and paper industries and in the medical field. Exposure to high doses and photoactivated MB has been found to have adverse effects to biological species [1].

For water pollution treatment, one of the most studied photocatalytic materials is zinc oxide (ZnO). Its relative large energy bandgap of 3.3 eV generates a sufficient number of electrons and holes upon illumination that facilitates the degradation of certain pollutants. The disadvantage of using ZnO by itself is that it corrodes under illumination [2], which limits its practical utilization. By synthesizing a ZnO-graphene composite, photocorrosion suppression of ZnO nanoparticles is achieved [3]. The surface hybridization of ZnO with carbon layers not only suppressed the photocorrosion but also enhanced the photocatalytic activity of the ZnO. They reported an 85% degradation of MB when irradiated with UV light for 75 minutes. Many reports have also shown improved photocatalytic performance using ZnO and graphene composites. An enhanced photocatalytic degradation of MB using reduced graphene oxide (rGO) and ZnO composite, synthesized via a simple one-pot hydrothermal method, was reported [4]. The method resulted in rGO sheets covering the ZnO flowers, resulting in the enhancement of photocatalysis as much as 97% with a rate

constant of 0.0395 min^{-1}. The enhancement was attributed to the decrease in the size of the ZnO flower and to the apparent interaction between the RGO sheets and the ZnO flowers. The limitation in potentially attaining maximum photocatalytic performance was the amount of rGO that can wrap the ZnO flowers.

The relationship between the size of the ZnO flower and the photocatalytic performance has also been reported [5]. The ZnO-rGO composite was synthesized also with a one-pot hydrothermal method by mixing ultrasonically exfoliated graphene oxide with an amine compound and an inorganic zinc compound in solution. This led to the sufficient removal of oxygen functionalities leaving graphene sheets, where the ZnO nanoparticles then grow. The results are comparable to the work described in the previous paragraph, owing to the synergistic interaction between the ZnO nanoflowers and the graphene and also to the high conduction of charges through graphene sheets.

In another work [6], G/ZnO nanocomposites were synthesized through a two-step electrochemical technique. Photocatalytic activity of the annealed G/ZnO was found to be improved as compared to ZnO and as-synthesized G/ZnO. Through the modified Kubelka–Munk function, energy band gaps have also been reported to be less than 3.37 eV. Similar to mentioned studies, enhanced photocatalytic activity was traced to the interaction of ZnO with graphene sheets.

Liu et al. [7] used one-pot hydrothermal synthesis of ZnO-reduced graphene oxide composites to study photocatalysis, by utilizing Zn powder as both reducing agent and precursor of ZnO and a surfactant, which reportedly promotes the reduction and dispersion of GO. They exhibited a MB degradation of 100% in 90 minutes for the ZnO-rGO composite, even without the use of the surfactant.

In this work, we utilized a one-pot chemical method for the synthesis of ZnO-reduced graphene oxide using zinc powder as a precursor without any thermal treatment. Such method has been used before for the development of supercapacitors [8, 9]. The method is simple and straightforward, does not require the use of any complex zinc precursors, and can be done at room temperature. We will also show that the oxidation of zinc and the simultaneous reduction of graphene oxide lead to a high-quality zinc oxide and reduced graphene oxide composite that acts as an excellent and highly efficient photocatalytic material. Furthermore, we will demonstrate that the bonding of zinc to the oxygen in graphene oxide and the synergistic effect between ZnO and the carbon layers is mainly responsible for the photocatalytic enhancement.

2. Materials and Methods

The method described below is simple and straightforward, requires relatively little processing time, and is easily scalable. It is also an environmentally friendly method as no thermal treatment was used to reduce the graphene oxide and no zinc compounds and inorganic compounds were used as zinc oxide precursors.

Graphene oxide (GO) was synthesized via modified Hummer's method [10]. It was then dispersed in 100 mL of distilled water (1.5 mg GO/mL H_2O) and ultrasonicated for 5 minutes to homogenize the dispersion. At ambient conditions, 100 mL of 6 weight % ammonia solution (Qualikems) was added and mixed with the GO suspension. Afterwards, zinc powder was slowly added to the suspension and mixed, in varying GO to Zn ratios. As the Zn powder (HiMedia) was added, the color of the suspension gradually changed from brown to black. This is a clear indication of the reduction of GO [9]. The samples were named ZG1, ZG2, ZG3, ZG4, and ZG5 corresponding to a Zn : GO mass ratio of 1 : 1, 2 : 1, 5 : 1, 10 : 1, and 20 : 1, respectively. The resulting mixture was then ultrasonicated for 1 hr. Subsequently, potassium hydroxide (KOH) pellets (RCI Labscan, 85%) were added to the suspension without stirring and left 24 hours at room temperature. The resulting precipitate was then filtered and washed with distilled water and ethanol (RCI Labscan, 99.9%), and the filtrates were dried in an oven at 60°C for 24 hrs.

Scanning electron microscopy with a JEOL JSM-6010 LV was used to study the morphology of the powder samples. The crystallinity and degree of reduction was analyzed with a Rigaku SmartLab 9 kW X-ray diffractometer with Cu Kα1 ($\lambda = 1.54056$ Å) at the National Institute for Material Science in Japan and Raman spectroscopy using an Argon laser source ($\lambda = 514.5$ nm) at the National Institute of Physics at the University of the Philippines, Diliman, Quezon City, Philippines.

The photocatalytic activity of the ZnO-rGO composites was evaluated by the decomposition of methylene blue (MB) (Ajax Finechem) under ultraviolet light. The reactor was prepared by adding 20 mg of the synthesized ZnO-rGO to 50 mL of MB (20 μM). Prior to UV irradiation, the solution has been stirred using a magnetic stirrer for 30 minutes in the dark to attain its adsorption-desorption equilibrium. Afterwards, the solution was irradiated with UV light with continuous magnetic stirring inside an aluminum foil-covered chamber. A commercially available UV light source (black light type) was used with an approximate power of 12 W. A Shimadzu UV-mini 1240 UV-Vis spectrophotometer was used to obtain the spectra of MB from 200 nm to 700 nm, beginning at the time when it achieved its adsorption-desorption equilibrium and every 30 minutes thereafter for two hours. At each time, 3 mL of the solution was collected from the reactor. This was done for all five samples of ZnO-rGO composites and for the GO sample.

3. Results and Discussion

3.1. Photocatalytic Degradation of Methylene Blue. Figure 1 shows the photocatalytic degradation of methylene blue (MB) by UV light using zinc oxide-reduced graphene oxide composite as a function of time.

For comparison, commercially available zinc oxide was also used in the experiment. To quantify the photocatalytic activity, the following expression for efficiency was used [11]:

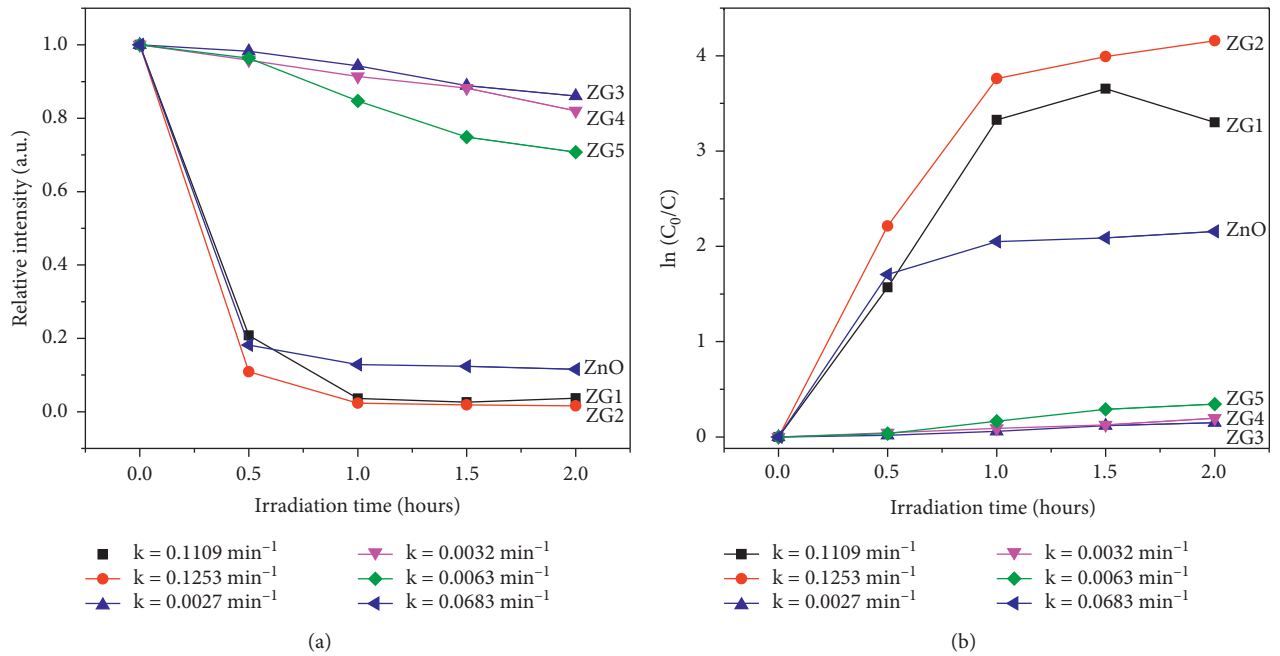

Figure 1: (a) Relative absorbance intensities of ZG1, ZG2, ZG3, ZG4, ZG5, and ZnO as a function of time of irradiation with UV light; (b) kinetic study of MB photodegradation with varying amounts of Zn : GO.

$$D(\%) = \left[1 - \frac{A_t}{A_0}\right] \times 100\%, \quad (1)$$

where A_0 is the absorbance of MB in the dark and A_t is the absorbance of MB under UV illumination for a time t (mins).

The absorbance of MB at 664 nm was used as reference for measuring the initial concentration of the solution. Throughout the tests, the absorbance peak of MB shifts to a lower wavelength which suggests dye degradation resulting in altered chemical composition. This change in the chemistry of the system is due to redox reactions facilitated by photogenerated holes and electrons. Table 1 shows the location of the absorbance peak of MB for each time interval.

The most efficient photocatalytic degradation of MB was observed with ZG2 having degraded 97.7% of the dye within one hour. To the best of our knowledge, this is a record efficiency for photocatalytic degradation of MB with ZnO-rGO composites synthesized through an environmentally friendly, low-cost, and highly-scalable method. The efficiency for sample ZG1 was nearly the same at 96.4% within one hour. After the first hour, samples ZG1 and ZG2 had very little response to UV illumination. There was a remarkable decrease in efficiency within one hour for ZG3, ZG4, and ZG5 considering that the zinc precursor content was significantly increased as compared to ZG1 and ZG2. Zn (4.534 m^2/g) [12] has a smaller effective surface area as compared to previously reported ZnO-graphene and ZnO-graphene oxide composites, with specific surface area ranging from 16 m^2/g to 158 m^2/g [13]. Increasing the amount of Zn precursor decreases the effective surface area of the samples, which in turn decreases the efficiency of the samples ZG3, ZG4, and ZG5 for photocatalysis.

Table 1: MB absorbance peak location for every time interval of UV irradiation.

Catalyst	MB absorption peak (nm)				
	0 hours	0.5 hour	1 hour	1.5 hours	2 hours
ZG1	664	664	664	662	645
ZG2	664	664	664	662	660
ZG3	664	664	664	664	664
ZG4	664	664	664	664	664
ZG5	664	664	664	664	664
ZnO	664	633	620	619	605

Moreover, in the work reported by Mills et al. [14] on photobleaching of methylene blue (MB) using TiO_2, they identified the absorbance peak for colorless leuco methylene blue (LMB) in aqueous solution at $\lambda = 262$ nm. In this study, they have observed a decrease in the intensity peaks of MB (660 nm and 292 nm) and an increasing intensity in the absorbance peak of LMB which, according to the authors, indicates the reduction of MB to LMB. In our study, no peak was recorded for LMB at any interval of UV irradiation. This indicates that MB underwent complete degradation. The complete absorbance spectra of MB for different samples are shown in Supplementary Figure 1S.

Using a first-order kinetic model relating the concentration to the reaction time as depicted in the following equation [15], the photocatalytic rate constant, k, was determined:

$$\ln\left(\frac{C_0}{C}\right) = kt. \quad (2)$$

The kinetic rates corresponding to each sample were obtained directly from a regression analysis of the linear

relation of ln (C_0/C) versus t, as shown in Figure 1(b). Sample ZG2 exhibited the highest rate constant followed closely by sample ZG1 (see the Supplementary Table 1S for the list of the rate constants for all samples). As the zinc precursor was increased further, the kinetic rate decreased considerably by forty times. This was followed by a gradual increase in the kinetic rate as more zinc metal was introduced.

It is interesting to observe that an efficient photocatalytic reaction was obtained at an optimum 33 wt% GO in sample ZG2. A previous investigation done by Xu et al. [4] showed that increasing the GO content from 1 wt% to 3 wt% enhances the photocatalytic degradation of MB to 95% in 80 minutes corresponding to a rate constant of 0.0395 min^{-1}. They attribute this achievement to the decreasing ZnO flower size with increasing GO content and to the electronic interaction between the reduced graphene oxide sheet and the ZnO flowers. However, their method prevents further photocatalytic degradation since rGO already covers the underlying ZnO flowers at 3 wt% GO. Following their results, increasing the GO content may lead to an increase in the kinetic rate and to further enhancement of photocatalytic performance. In our experiments, increasing the GO content was made possible by introducing the zinc metal onto the underlying GO substrate. However, the dependence of the photocatalytic efficiency to the GO content is counterintuitive. As the GO content was increased from 4.8 wt% (ZG5) to 9.1 wt% (ZG4) to 17 wt% (ZG3), the efficiency after 2 hours decreased from 29.2% to 18.0% to 13.9%, respectively.

The proposed mechanism is a combination of photodegradation and adsorption to rGO/GO sheets. As reported, methylene blue is strongly adsorbed on the GO surface [16]. The first few intervals of UV irradiation of MB solution using ZG1 and ZG2 was dominated by the adsorption of MB molecules on the photocatalyst, as indicated by the minimal redshift of the absorbance peak for MB but accompanied by a large difference in absorbance intensity. From these observations, a two-step photodegradation process for the degradation of MB is proposed. This mechanism shows two steps in the photodegradation of MB by ZG1 and ZG2: (1) adsorption of MB molecules on the catalyst and (2) reaction of hydroxyl radicals with MB molecules to decompose or degrade the dye. This proposed mechanism is in accordance with an earlier report where graphene sheet acts as new reaction sites [17].

3.2. Scanning Electron Micrographs. At low magnification (not shown), GO appears as compacted sheets. Upon closer inspection at a higher magnification, each GO sheet appears to be relatively smooth (Figure 2(a)). The surface of the zinc powder (Figure 2(b)) is also relatively smooth but contains smaller zinc particles. The SEM image of sample ZG2 (Figure 2(c)) shows a thin layer of rGO covering, which appears to be a zinc metal particle. Small rod-like structures, approximately 0.2 μm in diameter, appear on the rGO sheet. Even smaller particles are present on the surface of the zinc metal, which does not appear on the surfaces of the zinc powder. The morphology of sample ZG5 (Figure 2(d)) exhibits the same smaller particles present on the surface of the zinc powder in ZG2, as well as larger particles, which are presumably zinc oxide. There is no indication of any rGO found on these surfaces for ZG5.

3.3. X-Ray Diffractometry and Raman Spectroscopy Analysis. In order to understand the origin of the enhanced photocatalysis, we analyze the observations from XRD and Raman spectroscopy. Figure 3 shows the Raman spectra for all samples. Raman active peaks for both ZnO and GO can be observed in Figure 3(a). The most prominent peak at 426–429 cm^{-1} for zinc-containing samples ZG1 to ZG5 is attributed to the E2 (high) vibrational mode corresponding to vibrations along the oxygen sublattices [18]. The presence of this peak clearly indicates the formation of hexagonal wurtzite ZnO in all five samples, which agrees with the XRD results. The shift to lower wave numbers from the frequency of 437 cm^{-1} corresponding to the E2 (high) mode in bulk ZnO may be due to the effect of defects as a result of the finite size of the crystalline domain [18]. The peak at 575 cm^{-1} is also observed for all zinc-containing samples. This corresponds to the A1 longitudinal optical phonon mode for ZnO [A1(LO)].

Two more peaks are seen in Figure 3(a) that is also attributed to ZnO vibrational modes. The peak found in all samples between 329 and 333 cm^{-1} corresponds to the difference, E2 (high)–E2 (low) [19, 20]. The peak at 1140 cm^{-1} found in all samples, except ZG2 where it is found at 1129 cm^{-1}, is assigned to the second-order longitudinal optical phonon mode [2-LO] characteristics of II–IV semiconductors [21, 22] (see Supplementary Figure 2S for the Raman spectra of the samples for the range corresponding to ZnO vibrational modes). In general, the relative intensities of these peaks for ZnO relative to rGO follow an increasing trend with increasing zinc content for all samples except ZG2. In addition to the ZG2 redshift, there is an abrupt increase in relative intensity from ZG1 to ZG2 and then a decrease in relative intensity from ZG2 to ZG3. A study on the first- and second-order Raman spectra using density functional theory (DFT) [20] shows that the 2-LO phonon modes should be found at 1158 cm^{-1}.

All samples exhibited a redshift, as shown in Figure 4. It was suggested that the redshift might be due to the presence of defects and impurities. Since the relative intensity of the E2 (high) mode increased, the redshift cannot be attributed to intrinsic defects but rather implies the presence of extrinsic defects. Such redshift has been reported before in previous works where Mn was substituted for Zn [23] and Zr for Zn [24]. In this work, the anomalous behaviour exhibited by sample ZG2 may be similarly explained.

The Raman active peaks for GO are observed at 1359 cm^{-1} and 1603 cm^{-1} corresponding to the D- and G-bands, respectively [25–27]. The blue shift of the G-band from the ideal 1580 cm^{-1} for graphite corresponds to the formation of nanocrystalline graphite [28]. It is possible that the G and D' bands overlap. The D' band is associated with crystal defects [29]. Following the assumption that the G and

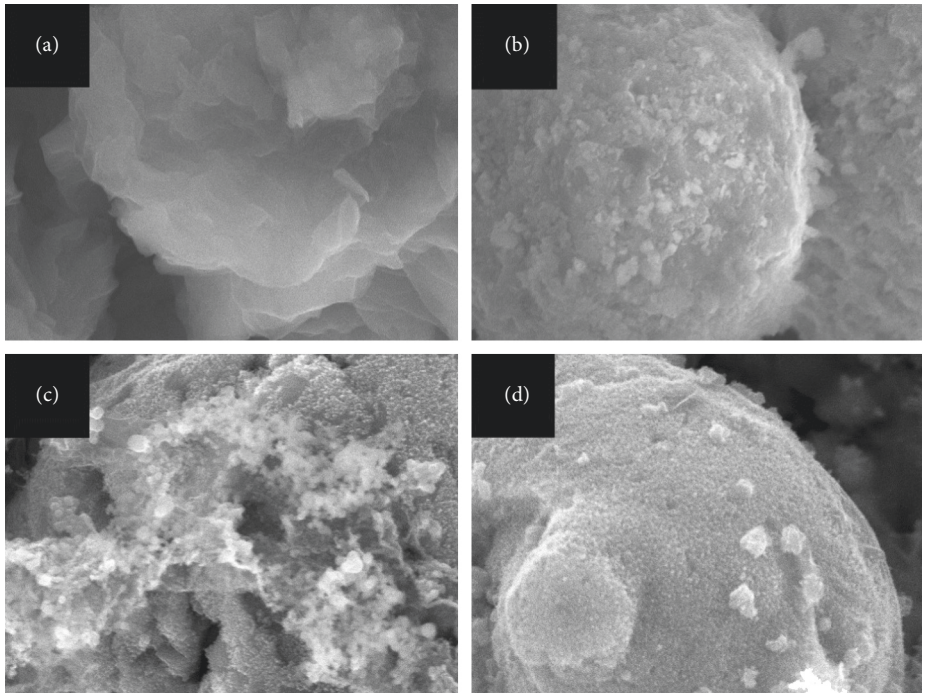

Figure 2: Scanning electron microscopy images of the surfaces of (a) graphene oxide (sample GO), (b) zinc metal, (c), sample ZG2, and (d) sample ZG5. The scale bars under each of the letters for (a) and (b) are 2 micrometers, while for (c) and (d) are 1 micrometer, in lengths.

D' bands overlap, then as zinc was added, the G-band shifted to lower frequencies with the peak at around 1577 cm^{-1}, while the D' band peak increases slightly to 1611 cm^{-1} for samples ZG1 to ZG4. The G and the D' band peaks then redshifts, respectively, to 1570 cm^{-1} and 1600 cm^{-1} for sample ZG5. The separation between the G and D' bands, shown in Figure 2(b), may be attributed to either strain on the graphene sheet [30, 31] or chemical doping [32, 33]. We also observe the presence of the 2D and S3 band peaks at 2685 cm^{-1} and 2930 cm^{-1}, respectively, for sample ZG1. The 2D peak, sometimes referred to as the G' peak, and the S3 peak are both associated with defects in graphene. These defects are due to the edges of the graphene planes as a result of the reduction of graphene oxide [25, 26], which is consistent with the SEM results.

The ratio of the intensities of the peaks of the D-band and G-band, i.e., I_D/I_G, describes the quality of graphene relative to the presence of in-plane defects. From ZG1 to ZG2, the ratio decreased implying an improved crystalline quality of graphene as the zinc content was increased twice. Increasing the zinc metal precursor further from ZG2 to ZG3 increases the intensity ratio indicating a decreased crystalline quality of graphene. As the zinc content was further increased from ZG3 to ZG5, the I_D/I_G ratio decreased. However, this does not necessarily mean improved crystallinity. As the zinc content was increased, the full-width at half maximum of the D-band increased and the intensities of the D- and G-bands relative to the zinc oxide peak intensities decreased. The most probable reason for this is that as the zinc metal precursor is increased, more and more zinc oxide is formed on the surface of the zinc metal that is covering the GO resulting in the decreased Raman response from the rGO sheets.

X-ray diffraction measurements were performed in order to confirm the presence of ZnO in our samples and to further study the reduction of graphene oxide. Figure 5 shows the characteristic peaks at 31.7°, 34.4°, 36.2°, 47.5°, and 56.5° for hexagonal wurtzite ZnO (JCPDS PDF Card 00-036-1451) corresponding to reflections from the 100, 002, 101, 102, and 110 planes. The peak at 56.5° corresponding to the 110 plane is observed to have a higher intensity for ZG4 which suggests that the thickness of ZnO is increased for this sample. The peaks were sharp suggesting the very good crystallinity of the synthesized zinc oxide, consistent with the Raman spectroscopy measurements.

The characteristic peaks for graphene oxide (GO) at around $2\theta = 9.8°$ and 19.2° for the 001 and 002 planes are also observed in Figure 5. The synthesized GO also contained a small amount of graphite, as evidenced by the peak at $2\theta = 42.1°$ [34]. This peak became less evident with increasing zinc content, indicating that the graphene sheets became functionalized.

The complete list of lattice parameters a and c for ZnO and the interlayer spacing for GO 001 and rGO was calculated using Bragg's equation and is shown in Table 2. The lattice constant decreased, as the zinc metal precursor is increased, approaching a value corresponding to that of single crystal ZnO. On the contrary, the lattice constant c has a maximum value for sample ZG2. This seems to suggest a direct chemical bond between the ZnO and GO, but this does not explain the increasing GO lattice spacing with increasing zinc content.

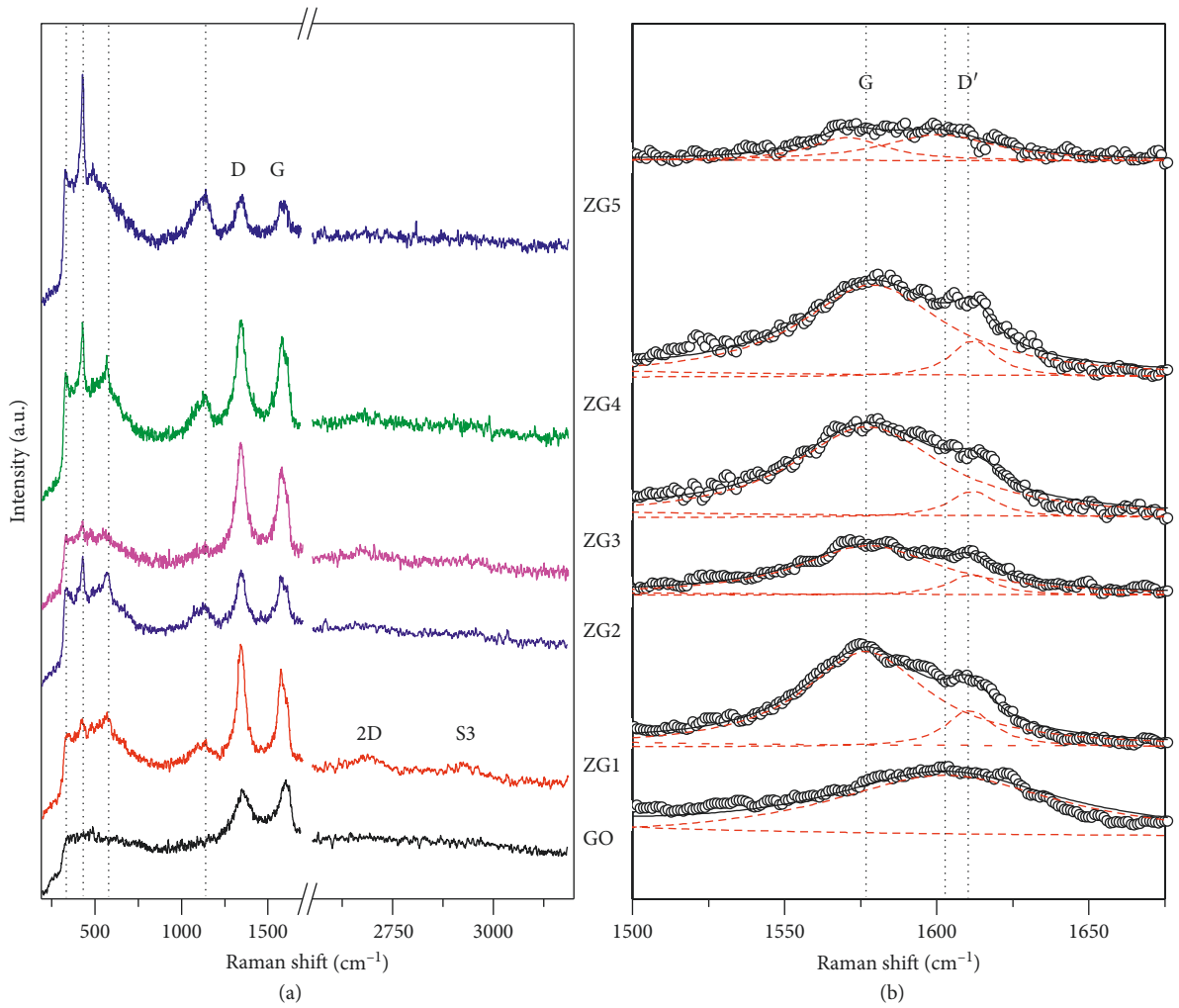

FIGURE 3: Raman spectroscopy measurements of samples GO, ZG1, ZG2, ZG3, ZG4, and ZG5 for (a) the full range from 200 cm^{-1} to 3300 cm^{-1} and (b) the range corresponding to the G-band.

4. Discussion

Three unusual behaviours in the reduction of GO are discussed. In typical reduction processes, such as thermal [35, 36], hydrothermal [7] or chemical [9, 16, 27], GO is completely reduced as indicated by the shift to higher values of a single characteristic 2θ peak. In this work, two sets of peaks are observed at around 6.9° to 8.6° and 23.7° to 24.2° in the spectra of samples ZG1 to ZG5. In general, the first set (peaks assigned with open circles) is attributed to GO but shifted towards lower values of 2θ with increasing zinc content. This implies a gradual increase in the interplanar spacing of the GO sheets from 9.05 Å to 12.26 Å. The second set (peaks assigned with closed circles) is ascribed to reduced graphene oxide (rGO), consistent with previous results [25, 37]. This is attributed to the formation of the graphene layers as a result of the breaking of the Van der Waals forces between graphene sheets in the composites and to the removal of oxygen functionalities and adsorbed water [9, 10, 34]. This supports the idea that Zn acts a reducing agent for GO.

The second atypical behaviour is the presence of a small peak at $2\theta = 13.0°$ for samples ZG2 and ZG3. This may be attributed to the presence of water intercalated between the GO sheets, which imply a partial reduction of the GO for these two samples [34]. The third is the abrupt increase of the GO interlayer spacing to 12.76 Å in sample ZG2. However, the presence of adsorbed water molecules between the GO sheets cannot explain this behaviour exhibited by sample ZG2 and the corresponding excellent photocatalytic activity in Figure 1.

As seen in Figure 1, ZG2 and ZG3 have an efficiency of 97.7% and 5.7%, respectively, after one hour. It is natural to expect that the efficiency should increase with increasing amount of zinc precursors. This discontinuous trend can be explained by taking note that as more zinc is added, more of the GO is covered with it. With a relatively small zinc content, ZnO is formed when zinc bonds with oxygen in GO.

The role of GO is important in the formation of ZnO, as evidenced the existence of the two XRD peaks corresponding to both GO and rGO. The oxygen in GO bonds with the zinc in the precursor results in the first 2θ peak, and

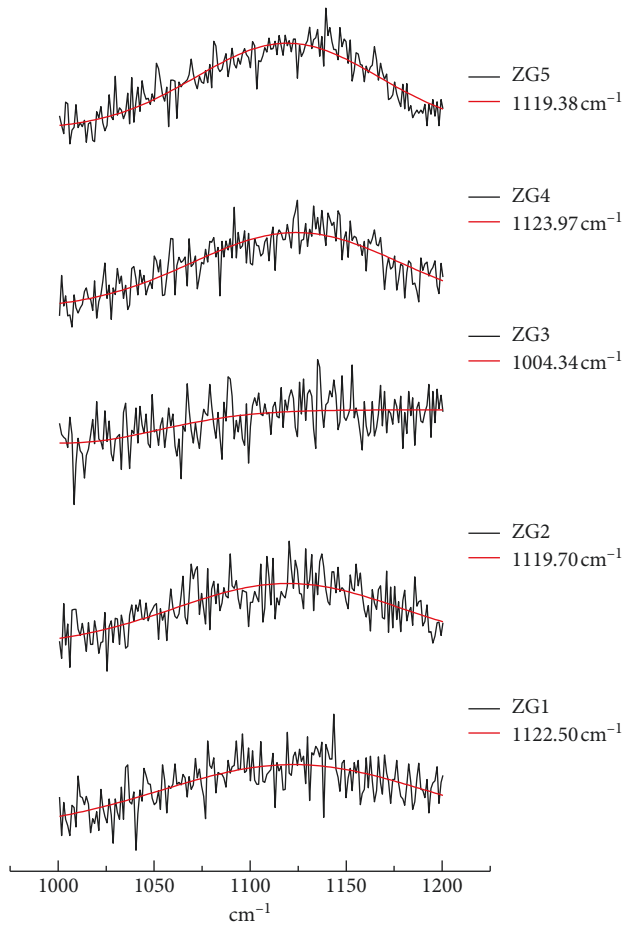

FIGURE 4: Raman spectroscopy measurements of samples ZG1, ZG2, ZG3, ZG4, and ZG5 for the range corresponding to the 2-LO phonon mode, showing a redshift from 1158 cm^{-1}.

the apparent reduction of GO results in the second 2θ peak. These two peaks are clearest in samples ZG1 and ZG2. The reason for the slightly reduced photocatalytic efficiency of sample ZG1 is due to the presence of defects as evidenced by the existence of the 2D and S3 Raman peaks and by the higher I_D/I_G ratio.

Raman measurements also show a ZnO phase decrease and GO phase increase with increasing relative GO content. Since the amount of GO was the same in all the samples, the decrease in the detection of the XRD reflections from the GO and rGO planes and of the Raman vibrational modes due to GO and rGO from ZG3 to ZG5 is attributed to increasing amount of zinc covering the underlying GO. The increased amount of zinc also led to an increased amount of ZnO, as exhibited in both Raman and XRD measurements. Furthermore, the 001 GO peak shifts slightly towards higher values of 2θ as the zinc content is decreased (Table 1). It can also be noticed that the ratio I_D/I_G in the Raman spectroscopy measurements increases with decreasing zinc content. This implies increasing number of defects with decreasing zinc metal precursor, which consequently decreased the probability of formation of ZnO. In addition, with high formation probability follows an increase in the interlayer spacing of GO.

These analyses suggest three things. The first is that the zinc chemically bonds with the oxygen on the surface of graphene forming the rGO. The idea that zinc oxide is formed through a chemical bond with oxygen-containing functional groups (OFGs) on graphene was first presented by Ma et al. [38]. The OFGs served as nucleation site for a ZnO crystallite. Eventually, each of the ZnO crystallites combines to form a ZnO film. In this experiment, zinc on the metal surface readily bonded with the OFGs, forming Zn-O-C. Secondly, the photocatalytic degradation of MB is primarily due to the effect of ZnO. We surmise that the presence of rGO only improves the degradation efficiency by presumably preventing electron-hole recombination. The third point is that the formation of the Zn-O-C bond greatly enhances the photocatalysis of ZnO. This speculation requires further investigation.

One possible disadvantage in mechanical mixing is that when ZnO is formed in the solution, it may not directly bind with graphene. The interaction of ZnO with graphene is perhaps more of a dipole-dipole interaction rather than a direct charge transfer. It has been shown that both Zn-terminated polar surface of ZnO induces a dipole in the charge distribution of graphene [39]. While previous works describing photocatalysis of ZnO-graphene composites show that is comparatively efficient with this work, the kinetic rate could benefit more from a direct charge transfer rather than charge induction. This hypothesis needs to be verified further through a more detailed experiment in the future.

The GO enhancing the photocatalytic activity of ZnO also hints toward a better material for dye-sensitized solar cells. The Zn-O-C bonding may yet prove to perform better in terms of electron transfer kinetics between the metal oxide and the conducting electrode. To verify whether there is an indication of such chemical bonds, we performed thermal gravimetry (TG) and differential thermal analysis (DTA) on sample ZG2 and compared it with the zinc metal powder used as the precursor and a commercially available ZnO. The results for the TG and DTA measurements are shown in Figure 6. All samples exhibited a mass loss below 100°C, which corresponds to the removal of water molecules. Two endothermic peaks can be observed in the DTA measurements for the zinc metal sample. Two endothermic peaks at 253°C and 428°C are attributed to the phase transformation of zinc from solid to liquid. After the second endothermic process, even as the temperature is increased, we observe no mass loss. Instead, an increase in the sample mass was detected starting at 600°C. This exothermic process may be attributed to the possible formation of ZnO. The ZnO sample did not show any significant weight loss. This is understandable due its very high melting point near 2000°C.

The exothermic peak exhibited at $T > 600$°C corresponds to the further crystallization of the hexagonal wurtzite phase. This is consistent with results from the existing literature [40]. The mass loss of about 11% for sample ZG2 between 100°C and 300°C corresponds to the phase transformation of zinc at 244°C and the combustion of GO. Previous reports have shown that the thermal reduction of GO is most efficient between 150°C and 200°C, leaving behind nearly

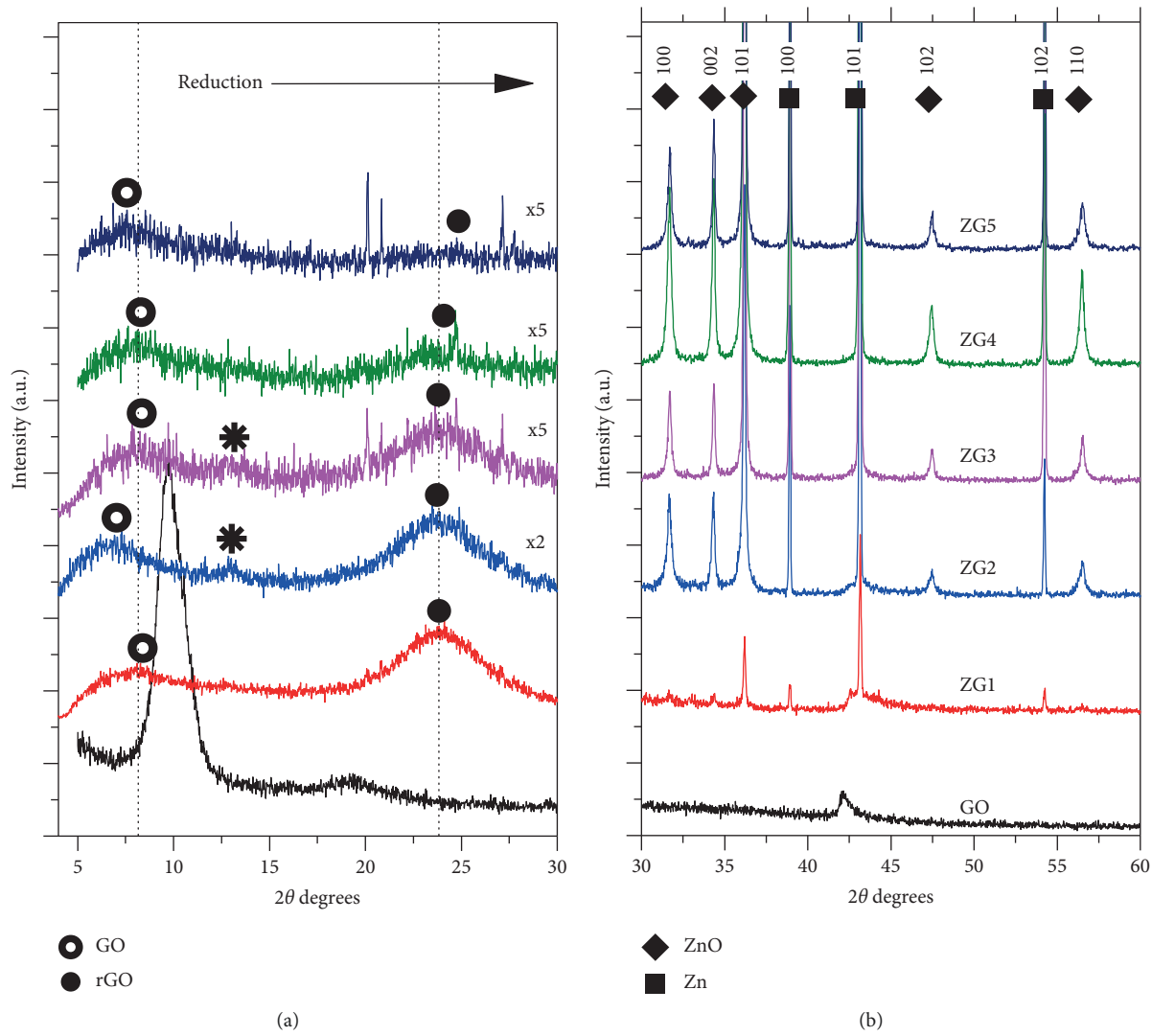

Figure 5: (a) The characteristic peaks for graphene oxide (⊙), reduced graphene oxide (●), and water intercalated between graphene sheets (*) with increasing zinc content are shown. The spectra for samples ZG2 to ZG5 have been magnified for clarity, as indicated by the numbers on the rightmost part. (b) The characteristic spectra for zinc oxide exhibit a hexagonal wurtzite structure. The peaks for zinc precursor are also present.

Table 2: The complete list of lattice parameters a and c for ZnO and the interlayer spacing for GO 001 and rGO.

Sample	a (Å)	c (Å)	c/a	dGO (Å)	drGO (Å)
GO				9.05	
ZG1	3.2613	5.2255	1.6023	11.04	3.68
ZG2	3.2594	5.2266	1.6005	12.76	3.73
ZG3	3.2554	5.2136	1.6015	11.32	3.74
ZG4	3.2554	5.2138	1.6015	11.55	3.75
ZG5	3.2514	5.2138	1.6036	12.26	3.74

crystalline carbon sheets with lattice defects [34]. Further increase in temperature exhibits the phase transition of zinc at 423°C and the combustion of carbon between 500°C and 600°C, which agree very well with literature [7]. At $T > 600$°C, the remaining 33% was zinc oxide, as indicated by the constant mass and the exothermic process leading to the crystallization of ZnO.

These results imply two things. First is that the reduction of GO resulted in the oxidation of zinc, as suggested by the remaining 33% ZnO. Sample ZG2 was synthesized with precursors composed of 67% zinc and 33% GO. The formation of ZnO, or presumably Zn-O-C, is therefore more favorable when GO is used as an oxidation substrate, compared to its formation in a basic solution. This interpretation supports previous work, where it was shown that GO acted as a nucleation seed and adhesion promotion agent for the formation of ZnO films [35]. Secondly, the idea that GO promotes ZnO formation in turn suggests that ZnO may be intercalated between graphene sheets, supported by XRD and Raman results.

Published work also suggests that the encapsulation of graphitic layers by ZnO suppresses the photocorrosion of ZnO [3]. The photocorrosion occurs when h^+ reacts with ZnO forming $Zn^{(2+)}$ and oxygen. With the carbon layers, the

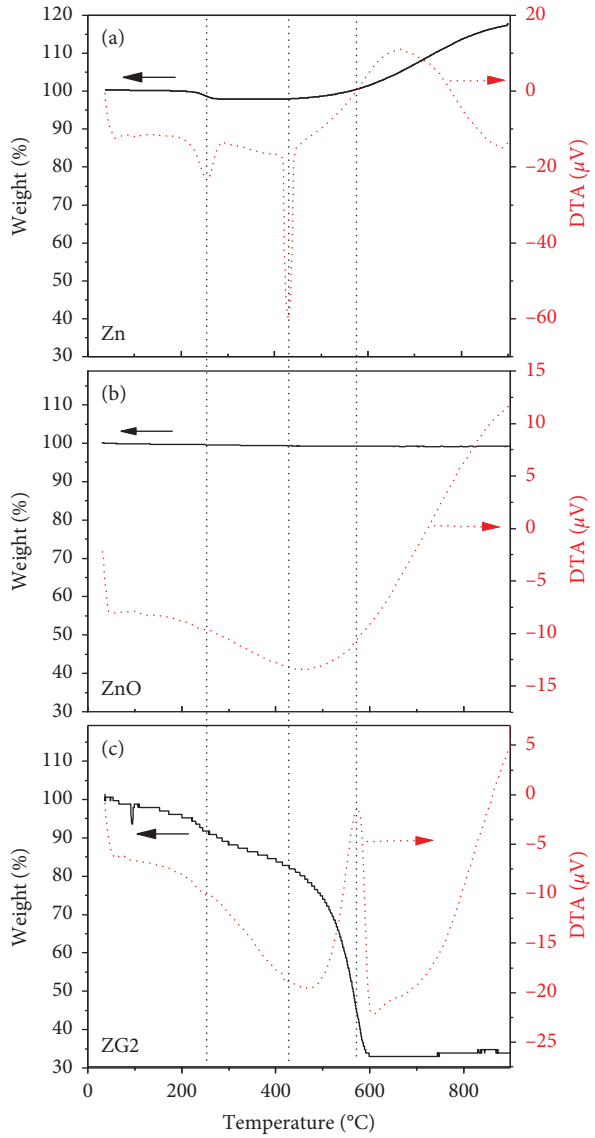

FIGURE 6: Comparative thermal gravimetry and differential thermal calorimetric (TG-DTA) measurements of samples Zn, ZnO, and ZG2.

MB molecules are strongly adsorbed. The photogenerated h^+ reacts with the adsorbed MB molecules and limits the photocorrosion of ZnO, due to the bonding of ZnO with the carbon layers. This resulted in the enhanced photocatalytic activity as exhibited in this present work.

5. Conclusions

We synthesized zinc oxide-reduced graphene oxide via one-pot chemical deposition using zinc powder as precursor at room temperature and characterized the photocatalytic performance of the composite. The most efficient photocatalytic degradation of MB was observed with sample ZG2 having degraded 97.7% of the dye within one hour, which corresponds to a kinetic rate of degradation of 0.125/min. To the best of our knowledge, this is a record efficiency for photocatalytic degradation of MB with ZnO-rGO composites. We argue that the possible formation of Zn-O-C and the synergistic interaction between ZnO and the graphene layers led to the enhancement of photocatalytic performance.

Data Availability

The characterization data and experimental results used to support the findings of this study are included within the article and in the supplementary file.

Disclosure

The abstract of this paper has been submitted at http://phantomsfoundation.com/GRAPHENECONF/2017/Abstracts/Grapheneconf2017_Agulo_Ian_Jasper_471.pdf.

Conflicts of Interest

The authors declare that there are no conflicts of interest regarding the publication of this paper.

Acknowledgments

This research was funded by the National Research Council of the Philippines (NRCP) (I-97).

Supplementary Materials

Figure 1S. Absorbance spectra of MB using (a) ZG1, (b) ZG2, (c) ZG3, (d) ZG4, and (e) ZG5 for different UV irradiation time intervals. Table 1S. Photocatalytic rate constant (k) of ZnO and ZnO-reduced graphene oxide composites on photodegradation of methylene blue (MB). Figure 2S. Raman spectroscopy measurements of samples GO, ZG2, ZG3, ZG4, and ZG5 for the range corresponding to ZnO vibrational modes. (*Supplementary Materials*)

References

[1] IARC Working Group on the Evaluation of Carcinogenic Risks to Humans, *Some Drugs and Herbal Products. IARC Monographs on the Evaluation of Carcinogenic Risks to Humans*, Vol. 108, International Agency for Research on Cancer, Lyon, France, 2016.

[2] P. Spathis and I. Poulios, "The corrosion and photocorrosion of zinc and zinc oxide coatings," *Corrosion Science*, vol. 37, no. 5, pp. 673–680, 1995.

[3] L. Zhang, H. Cheng, R. Zong, and Y. Zhu, "Photocorrosion suppression of ZnO nanoparticles via hybridization with graphite-like carbon and enhanced photocatalytic activity," *The Journal of Physical Chemistry C*, vol. 113, no. 6, pp. 2368–2374, 2009.

[4] S. Xu, L. Fu, T. S. H. Pham, A. Yu, F. Han, and L. Chen, "Preparation of ZnO flower/reduced graphene oxide composite with enhanced photocatalytic performance under sunlight," *Ceramics International*, vol. 41, no. 3, pp. 4007–4013, 2015.

[5] H. R. Pant, C. H. Park, P. Pokharel, L. D. Tijing, D. S. Lee, and C. S. Kim, "ZnO micro-flowers assembled on reduced graphene sheets with high photocatalytic activity for removal of pollutants," *Powder Technology*, vol. 235, pp. 853–858, 2013.

[6] A. R. Nanakkal and L. K. Alexander, "Photocatalytic activity of graphene/ZnO nanocomposite fabricated by two-step electrochemical route," *Journal of Chemical Sciences*, vol. 129, no. 1, pp. 95–102, 2017.

[7] G. Liu, M.-J. Liu, and Y.-J. Liu, "A novel fuzzy control algorithm of hybrid digital signal processing," *Advances in Mechanical and Electronic Engineering*, vol. 229, pp. 533–539, Springer, Berlin, Germany, 2013.

[8] Y. Liu, Y. Li, M. Zhong, Y. Yang, Y. Wen, and M. Wang, "A green and ultrafast approach to the synthesis of scalable graphene nanosheets with Zn powder for electrochemical energy storage," *Journal of Materials Chemistry*, vol. 21, no. 39, pp. 15449–15455, 2011.

[9] Y.-Z. Liu, Y.-F. Li, Y.-G. Yang, Y.-F. Wen, and M.-Z. Wang, "A one-pot method for producing ZnO-graphene nanocomposites from graphene oxide for supercapacitors," *Scripta Materialia*, vol. 68, no. 5, pp. 301–304, 2013.

[10] W. S. Hummers, Jr., and R. E. Offeman, "Preparation of graphitic oxide," *Journal of the American Chemical Society*, vol. 80, no. 6, p. 1339, 1958.

[11] M. Sookhakian, Y. M. Amin, and W. J. Basirun, "Hierarchically ordered macro-mesoporous ZnS microsphere with reduced graphene oxide supporter for a highly efficient photodegradation of methylene blue," *Applied Surface Science*, vol. 283, pp. 668–677, 2013.

[12] A. H. Abbar, S. A. Rushdi, and H. M. Al-Tameemi, "Electrochemical preparation of ultrafine zinc powder," *International Journal of Electrochemical Science*, vol. 12, pp. 7075–7088, 2017.

[13] P. Raizada, A. Sudhaik, and P. Singh, "Photocatalytic water decontamination using graphene and ZnO coupled photocatalysts: a review," *Materials Science for Energy Technologies*, vol. 2, no. 3, pp. 509–525, 2019.

[14] A. Mills and J. Wang, "Photobleaching of methylene blue sensitised by TiO_2: an ambiguous system?" *Journal of Photochemistry and Photobiology A: Chemistry*, vol. 127, no. 1–3, pp. 123–134, 1999.

[15] A. Molla, Y. Li, B. Mandal, S. G. Kang, S. H. Hur, and J. S. Chung, "Selective adsorption of organic dyes on graphene oxide: theoretical and experimental analysis," *Applied Surface Science*, vol. 464, pp. 170–177, 2019.

[16] D. Fu, G. Han, Y. Chang, and J. Dong, "The synthesis and properties of ZnO-graphene nano hybrid for photodegradation of organic pollutant in water," *Materials Chemistry and Physics*, vol. 132, no. 2-3, pp. 673–681, 2012.

[17] Y. Li, X. Li, J. Li, and J. Yin, "Photocatalytic degradation of methyl orange by TiO_2-coated activated carbon and kinetic study," *Water Research*, vol. 40, no. 6, pp. 1119–1126, 2006.

[18] H. Morkoç and Ü. Özgür, *Zinc Oxide—Fundamentals, Materials and Device Technology*, Wiley-VCH Verlag GmbH & Co. KGaA, Weinheim, Germany, 2009.

[19] C. F. Klingshirn, B. K. Meyer, A. Waag, A. Hoffman, and J. Geurts, *Zinc Oxide—from Fundamental Properties towards Novel Applications*, Springer-Verlag, Berlin, Germany, 2010.

[20] R. Cuscó, E. Alarcón-Lladó, J. Ibáñez, J. Artús, L. Wang, and M. J. Callahan, "Temperature dependence of Raman scattering in ZnO," *Physical Review B*, vol. 75, no. 16, Article ID 165202, 2007.

[21] C. A. Arguello, D. L. Rousseau, and S. P. S. Porto, "First-order Raman effect in wurtzite-type crystals," *Physical Review*, vol. 181, no. 3, pp. 1351–1363, 1969.

[22] K. A. Alim, V. A. Fonoberov, M. Shamsa, and A. A. Balandin, "Micro-Raman investigation of optical phonons in ZnO nanocrystals," *Journal of Applied Physics*, vol. 97, no. 12, Article ID 124313, 2005.

[23] L. N. Dem'yanets, R. M. Akalyukin, and B. N. Mavrin, "Growth and Raman spectra of doped ZnO single crystals," *Inorganic Materials*, vol. 47, no. 6, pp. 649–653, 2011.

[24] S. Vojisavljevic, M. Sreckovic, M. Grujic-Brojcin, T. Srećković, Z. Brankovic, and G. Brankovic, "Structural characterization of mechanically milled ZnO: influence of zirconia milling media," *Journal of Physics: Condensed Matter*, vol. 20, no. 47, Article ID 475202, 2008.

[25] V. Strong, S. Dubin, M. F. El-Kady, A. Lech, Y. Weiller, and R. B. Kaner, "Patterning and electronic tuning of laser scribed graphene for flexible all-carbon devices," *ACS Nano*, vol. 6, no. 2, pp. 1395–1403, 2012.

[26] T. V. Cuong, V. H. Pham, Q. T. Tran et al., "Optoelectronic properties of graphene thin films prepared by thermal reduction of graphene oxide," *Materials Letters*, vol. 64, no. 6, pp. 765–767, 2010.

[27] I. K. Moon, J. Lee, R. S. Ruoff, and H. Lee, "Reduced graphene oxide by chemical graphitization," *Nature Communications*, vol. 1, no. 1, p. 73, 2010.

[28] A. C. Ferrari and J. Robertson, "Interpretation of Raman spectra of disordered and amorphous carbon," *Physical Review B*, vol. 61, no. 20, pp. 14095–14107, 2000.

[29] X. Zhao and Y. Ando, "Raman spectra and X-ray diffraction patterns of carbon nanotubes prepared by hydrogen arc discharge," *Japanese Journal of Applied Physics*, vol. 37, no. Part 1, No. 9A, pp. 4846–4849, 1998.

[30] M. A. Bissett, M. Tsuji, and H. Ago, "Strain engineering the properties of graphene and other two-dimensional crystals," *Physical Chemistry Chemical Physics*, vol. 16, no. 23, pp. 11124–11138, 2014.

[31] O. Frank, M. Mohr, J. Maultzsch et al., "Raman 2D-band splitting in graphene: theory and experiment," *ACS Nano*, vol. 5, no. 3, pp. 2231–2239, 2011.

[32] M. Bruna and S. Borini, "Observation of RamanG-band splitting in top-doped few-layer graphene," *Physical Review B*, vol. 81, no. 12, Article ID 125421, 2010.

[33] K. Park and S. Ryu, "Direction-controlled chemical doping for reversible G-phonon mixing in ABC trilayer graphene," *Scientific Reports*, vol. 5, no. 1, p. 8707, 2015.

[34] T. N. Blanton and D. Majumdar, "X-ray diffraction characterization of polymer intercalated graphite oxide," *Powder Diffraction*, vol. 27, no. 2, pp. 104–107, 2012.

[35] Q. Pan, C.-C. Chung, N. He, J. L. Jones, and W. Gao, "Accelerated thermal decomposition of graphene oxide films in air via in situ X-ray diffraction analysis," *The Journal of Physical Chemistry C*, vol. 120, no. 27, pp. 14984–14990, 2016.

[36] Z. Hu, Y. Chen, Q. Hou, R. Yin, F. Liu, and H. Chen, "Characterization of graphite oxide after heat treatment," *New Journal of Chemistry*, vol. 36, no. 6, pp. 1373–1377, 2012.

[37] L. Fu, G. Lai, H. Zhang, and A. Yu, "One-pot synthesis of multipod ZnO-carbon nanotube-reduced graphene oxide composites with high performance in photocatalysis," *Journal of Nanoscience and Nanotechnology*, vol. 15, no. 6, pp. 4325–4331, 2015.

[38] Q. Ma, X. Zhu, D. Zhang, and S. Liu, "Graphene oxide—a surprisingly good nucleation seed and adhesion promotion agent for one-step ZnO lithography and optoelectronic applications," *Journal of Materials Chemistry C*, vol. 2, no. 42, pp. 8956–8961, 2014.

[39] K. Larson, A. Clark, A. Appel, Q. Dai, H. He, and S. Zygmunt, "Surface-dependence of interfacial binding strength between

zinc oxide and graphene," *RSC Advances*, vol. 5, no. 81, pp. 65719–65724, 2015.

[40] H. Farag, Z. M. Hanafi, M. Dawy, and A. E. Aziz, "Characterization of ZnO nanopowders synthesized by the direct precipitation method," *Canadian Journal of Pure and Applied Science*, vol. 4, pp. 1303–1309, 2010.